Progress in Oceanography 124 (2014) 54–65

Contents lists available at ScienceDirect

Progress in Oceanography

journal homepage: www.elsevier.com/locate/pocean

Signatures of the late Holocene Neoglacial cold event and their marine–terrestrial linkage in the northwestern Pacific margin

So-Young Kim [a], Dhong-il Lim [b,*]

[a] Arctic Research Center, Korea Polar Research Institute, Incheon 406-840, Republic of Korea
[b] South Sea Research Institute, Korea Institute of Ocean Science and Technology, Geoje 656-830, Republic of Korea

ARTICLE INFO

Article history:
Received 2 February 2013
Received in revised form 19 March 2014
Accepted 23 March 2014
Available online 1 April 2014

ABSTRACT

Marine microfossil assemblages in core sediments from the northern East China Sea (ECS) were investigated to understand late Holocene paleoclimatic changes in the northwestern Pacific margin. We find a pronounced alternation of ocean condition during the late Holocene characterized by an abrupt decrease in dinoflagellate cysts and Kuroshio water species of planktonic foraminifera centered at *ca.* 4000–2500 ^{14}C yr BP. Compilation and merger of new and previously published data show that this oceanic event corresponds with terrestrial cooling and dry episodes in the northern China. The synchronicity between marine and terrestrial records is considered to be linked to a weakened Kuroshio influence that is in coupled with intensified winter monsoon, highlighting a significance of oceanic-atmospheric dynamics in determining moisture and heat distribution over both oceanic and terrestrial domains. Superimposed on the late Holocene, the synchronicity between this particular climatic shift in the northwestern Pacific and the Neoglacial cold events in the northern high-latitude regions is tentatively indicative of a global climate signal, possibly associated with dynamics of the North Pacific gyre system and the high latitude North Atlantic thermohaline circulation, and therefore positions of the mean latitude of the Kuroshio extension.

Introduction

The marginal seas of the northwestern Pacific (e.g., Yellow Sea and East China Sea) are an important paleoclimate archive recording a wide variety of geologic and climatic processes in this area. As a transition between the world's largest continent and its ocean, these marginal seas contain sedimentary sequences that often provide detailed information regarding the evolution of continent-ocean-climate interactions through time (e.g., Ijiri et al., 2005; Li et al., 2007). Furthermore, understanding the climate systems of this region is particularly important, because it has strong societal relevance to the surrounded countries and worldwide. The East China Sea (ECS) is an open marginal sea in the northwestern Pacific and is considered to be a large source and reservoir of energy and materials originating from both land and ocean. The Kuroshio Current (KC), which covers the ECS shelf, is the main western boundary current of the northwestern Pacific. It is known to be a key component of the Asian climate system through the meridional transport of water mass, heat and freshwater, strongly affecting the climatic evolution of the adjacent continent, as well as ocean systems in the ECS shelf (e.g., An et al., 2000; Liu et al., 2007; Xiang et al., 2007). Several lines of evidence suggest that paleoceanographic records from the ECS region can provide insight into the evolution of regional climate and hydrographic conditions in the western Pacific near East Asia (e.g., Lin et al., 1996; Li et al., 2007; Chang et al., 2008).

Research has revealed that much of the Holocene period can be characterized by abrupt, small-magnitude climatic fluctuations (e.g., Bond et al., 1997; Xiang et al., 2007; Yoo et al., 2009). Millennial-scale climate oscillations during the Holocene are well recorded in proxy records such as ice-rafted debris events in the subpolar North Atlantic (Bond et al., 1997, 2001), cooling events in the subtropical North Atlantic off West Africa (deMenocal et al., 2000; Marret et al., 2006) and Arabian Sea (Sirocko et al., 1996), and reduced rainfall episodes in Oman (Neff et al., 2001) and Dongge Cave in China (Dykoski et al., 2005; Wang et al., 2005). Of particular interest is a discernible climatic signature of the late Holocene recorded in northern China and the East and South China seas, being generally characterized by cooler and drier climatic conditions (Jin et al., 2004; Xiang et al., 2007). However, an integrated perspective for marine and terrestrial sequences in this region has been lacking, although it is of primary importance to understand mechanisms transferring such climatic variability between both domains.

Microfossil assemblages preserved in the sedimentary record have been widely applied in paleoceanographic and paleoclimatic

* Corresponding author. Tel.: +82 55 639 8580; fax: +82 55 639 8509.
E-mail address: oceanlim@kiost.ac (D.-i. Lim).

http://dx.doi.org/10.1016/j.pocean.2014.03.010
0079-6611/

studies. For example, the abundance and species composition of planktonic foraminifera in marine sediments are useful tools for reconstructing past surface-water hydrography (e.g., Gupta et al., 2006; Xiang et al., 2007), since the distributions of modern planktonic foraminifera are known to be controlled by water mass and circulation patterns as well as upwelling and biological productivity (Bé and Tolderlund, 1971; Hemleben et al., 1998). Additionally, major shifts in benthic foraminiferal communities have been used to identify changes in depositional environments (e.g., Lim et al., 2006; Kang et al., 2010) as well as bottom-water salinity (e.g., Kim and Kucera, 2000; Xiang et al., 2008). Over the last decade, the use of dinoflagellate cysts for reconstructing paleoceanographic and paleoenvironmental conditions has been increased in parallel with an improvements in our understanding of modern dinoflagellate cyst distributions in relation to environmental parameters (e.g., Marret and Zonneveld, 2003; Matthiessen et al., 2005; de Vernal and Marret, 2007; Kim et al., 2010).

In this study, microfossil assemblages in sediment cores from the northern ECS were investigated and compared with existing marine and terrestrial records in order to identify a mechanism transferring the late Holocene climate fluctuations between marine and terrestrial environments in the northwestern Pacific margin.

Environmental setting

The ECS is one of the marginal seas of the western Pacific Ocean, bounded on the east by Ryukyu Islands, on the south by the island of Taiwan, and on the west by mainland China and the Asian continent (Fig. 1). It is connected to the South China Sea by the Taiwan Strait and with the East/Japan Sea by the Korea Strait, and it opens in the north to the Yellow Sea. The northwestern part of the ECS is characterized by a wide continental shelf with depths shallower than 200 m. The southeastern part of the ECS is occupied by the Okinawa Trough along the outer edge of the continental shelf that reaches up to *ca.* 2700 m in water depth (Zhang and Su, 2006).

The hydrography of the ECS is largely influenced by the KC, which originates from the North Pacific Equatorial Current. The KC enters the ECS along the east side of Taiwan and then flows into the Pacific through the south of Kyushu, Japan. A branch of the KC intrudes to the East Sea through the Korean/Tsushima Strait between Korea and Kyushu. Since the KC waters are warm (about 20 °C) and have relatively high salinities (about 34), it transports a large amount of heat and moisture from the tropics to the middle latitudes as it flows along the western edge of North Pacific (Hsueh, 2000; Ichikawa and Chaen, 2000). The northwestern part of the ECS is governed by coastal waters with lower temperatures and salinity under influences of two large rivers, the Yangtze River (Changjiang) and Yellow River (Huanghe). These rivers discharge a large amount of fresh water and terrestrial materials into the ECS, and their large nutrient input supports high primary production in the surface waters (Hama et al., 1997).

Sea surface temperature (SST) and salinity of the ECS are also regulated by the East Asian monsoons. The observed mean annual SST of the ECS is ~24.7 °C, with a seasonal range between ~28.6 °C (July) and ~21.8 °C (January). Mean annual sea surface salinity (SSS) is ~34.4, with a summer low of ~34.1 and a winter high of

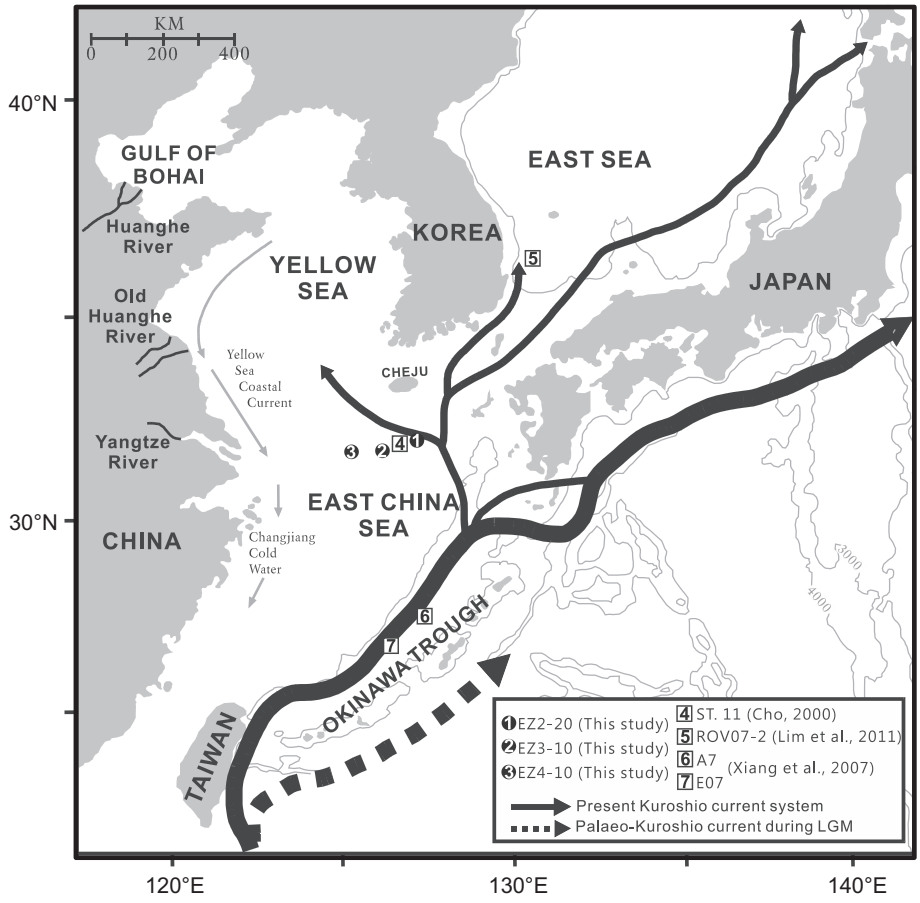

Fig. 1. The map showing the study area with the location of three piston cores collected for this study and previous reported cores, as well as the main path of the Kuroshio Current in the northwestern Pacific marginal seas. Black arrows indicate the Kuroshio Current and its branches (after Ujiié et al., 2003).

~34.7 (NOAA, 1994). During the summer, southerly winds bring warm, humid air and associated precipitation from low-latitude oceans to northeastern Asia and the adjacent seas, resulting in a large amount of freshwater discharge into the ECS. By contrast, during the winter monsoon, strong northerly winds bring cold, dry air from north-central Asia to the continent, reducing river discharge during these months (Chang et al., 2008).

Material and methods

Three sediment cores (EZ2-20, EZ3-10, and EZ4-10) were collected from the ECS continental shelf, located under the path of the KC, at water depths of 110, 65, and 50 m, respectively (Fig. 1). The cores were split lengthways, photographed, and logged. Details of sedimentary structures from some representative core sections were collected using X-ray radiographic photography. Grain-size analysis was conducted using a standard dry-sieving technique for the sand fraction (>4ϕ) and by a pipette method for the mud fraction (<4ϕ).

For dinoflagellate cyst analysis, cores EZ3-10 and EZ4-10 were subsampled at approximately 10-cm intervals. Approximately 5 g of subsamples were taken and treated following the method described by Cho and Matsuoka (1999). To prevent dinoflagellate cysts from being damaged by the oven-drying process, the original sample was divided into two parts: one was used to measure water content and the other was used for microscope analysis. To measure water content, the first half-sample was weighed wet and then oven dried at 70 °C for a day and reweighed; the weight difference was equivalent to the volume of lost water. The second half-sample was also weighed wet and then treated with *ca.* 50 ml of 10% hydrochloric acid (HCl) to remove calcium carbonate. Silicate materials were removed by applying *ca.* 50 ml of 47% hydrofluoric acid (HF) for about 24 h. After decanting and neutralizing with distilled water, the chemically treated samples were sonicated for 30 s and passed through 125 and 20 μm pore sized mesh sieves. Where possible, 300 dinoflagellate cysts were counted and identified from each sample with an inverted microscope (Nikon- Eclipse 55i) at 400 and 600 times magnification. Dinoflagellate cyst concentration in each sample was calculated as cysts/g dry weight of sediment: $N/W \times (1 - R)$, where N is a counted cyst number, W is a weight of an observed sediment, and R is a rate of water content of the sediment.

Analysis of planktonic foraminiferal assemblages was carried out on a total of 34 subsamples of EZ02-20 core sediment at approximately 10-cm intervals. The samples were oven-dried at 50 °C, weighed, and then washed through a 63-μm Tyler screen to separate the mud and sand fractions. After further drying, the material was reweighed and the >63 μm fraction was dry-sieved through a 150-μm screen. The resultant residue was divided into workable aliquot parts using a microsplitter to ensure consistency in the splitting the samples. At least 200 planktonic foraminiferas per sample were counted per sample and identified using a light microscope. For age dating and calculation of the relative ratio (%) between planktonic and total foraminifera abundance (P/T ratio), the benthic foraminifera in samples were counted and picked, but not identified.

Accelerator mass spectrometry (AMS) ^{14}C dating was performed on benthic foraminiferal tests (mixed species) and organic particles selected from a total of 16 horizons in cores EZ2-20, EZ3-10, and EZ4-10. AMS ^{14}C measurements were conducted at Beta Analytic, Inc. (Miami, FL, USA) and a 129-year reservoir age correction was applied (Kong and Lee, 2005). AMS ^{14}C ages of core samples are listed with the locations of cores in Table 1.

Results

Sediment characteristics and radiocarbon ages

The sediments of core EZ2-20 were mostly composed of greenish gray (5GY 2/1), homogeneous mud or muddy sand facies that displayed some bioturbation, as well as laminated sand/mud facies. The latter facies was particularly evident in the lower part of the core where the sediment showed a broad range of grain sizes of 2 to 8ϕ because of the well-developed sand and mud laminations (Fig. 2). The radiocarbon ages of core EZ2-20 measured at depths of 30, 100, 200, 350, and 450 cm were 2860 ± 40, 7,090 ± 40, 7140 ± 40, 12,560 ± 40, and 16,120 ± 140 ^{14}C yr BP, respectively (Table 1). The sedimentary analysis and the radiocarbon dates of the core suggest that the core yields a complete depositional sequence since the LGM (Last Glacial Maximum). Sediments of core EZ3-10 are an olive graish (5Y 4/2) and homogeneous mud facies with a mean grain size ranging from 8 to 9ϕ (Fig. 2). Silt and clay contents ranged from 29–42% and 52–70%, respectively, with minor amounts of sand (<10%). The radiocarbon ages at core depths of 20, 80, 200, 250, and 298 cm were 890 ± 40, 1630 ± 40, 1860 ± 40, 2160 ± 40, and 2470 ± 50 ^{14}C yr BP, respectively. These ages show that the sediments were continuously deposited since the late Holocene. Core EZ4-10 sediments, which were similar to those of EZ02-20 in sediment texture and sedimentary sturucture, were mainly dark olive gray (5Y 3/2), bioturbated and homogeneous sandy mud facies. Mean grain size varied between 5 and 8ϕ with sand contents varying between 10% and 40%, except for the lowermost section (below a core depth of 400 cm) with well-developed rhythmic sand/mud laminations.

Table 1
AMS ^{14}C age data for cores EZ2-20, EZ3-10 and EZ4-10 from the study area.

Core No.	Core depth (cm)	Measured ^{14}C age (yr BP)	Error (±year)	Conventional ^{14}C age (yr BP)	Error (± year)	Materials	Laboratory Ref. No.
EZ2-20	30	2406	40	2860	40	benthic foraminifera	Beta198576
	100	6700	40	7090	40	benthic foraminifera	Beta198578
	200	6740	40	7140	40	benthic foraminifera	Beta198579
	350	12,650	40	12,560	40	peat	Beta203467
	450	16,080	140	16,120	140	organic sediment	Beta203468
	20	500	40	890	40	benthic foraminifera	Beta204935
EZ3-10	80	1240	40	1630	40	benthic foraminifera	Beta204936
	200	1470	40	1860	40	benthic foraminifera	Beta204937
	250	1780	40	2160	40	benthic foraminifera	Beta-221825
	298	2070	40	2470	40	benthic foraminifera	Beta204938
	90	1460	40	1840	40	benthic foraminifera	Beta221827
EZ4-10	210	2180	40	2570	40	benthic foraminifera	Beta204941
	365	3960	40	4350	40	benthic foraminifera	Beta204942
	480	22,410	130	22,450	130	organic sediment	Beta207360
	510	25,000	190	25,020	190	organic sediment	Beta207361

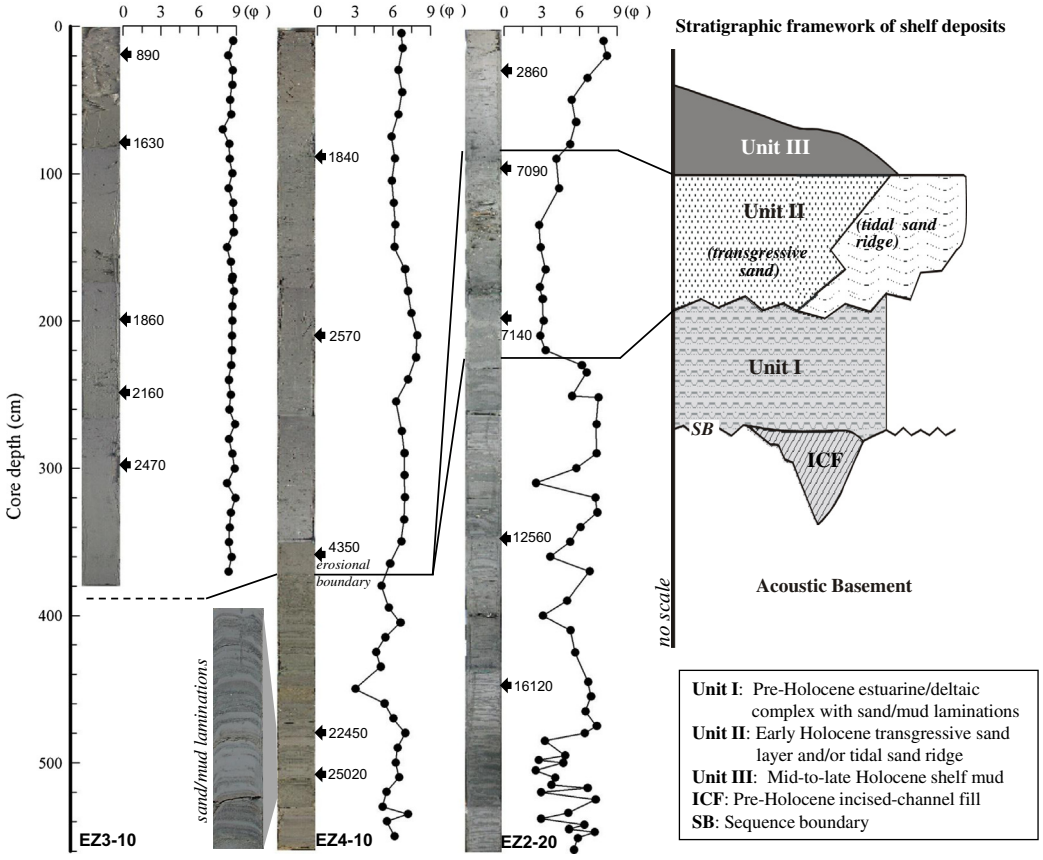

Fig. 2. Stratigraphic correlation of three cores from the study area and late Pleistocene stratigraphic framework of northern East China Sea shelf deposits (after Yoo et al., 2002). Numbers with arrows are radiocarbon ages (^{14}C yr BP).

The radiocarbon ages at core depths of 90, 210, 365, 480, and 510 cm were 1840 ± 40, 2570 ± 40, 4350 ± 40, 22,450 ± 50, and 25,020 ± 50 ^{14}C yr BP, respectively. Of particular note is the considerable age gap at *ca.* 380 cm depth of the core (Fig. 2). This suggests that a strong erosional process affected the study site during the post-glacial transgression period, followed by resedimentation at 6000–5000 ^{14}C yr BP when the sea level neared its present level (e.g., Kong et al., 2006).

Considering the ^{14}C age dating and lithologic characters of the cores, together with geochemical, micropaleontological, and seismic stratigraphic data of several previous studies (Lim et al., 2000; Yoo et al., 2002; Hyun et al., 2006; Rho, 2009; Kang et al., 2010), the integrated evolution history of core sediments from the northern shelf of ECS can be divided into three stages, separated by sharp lithologic changes bounded by erosional surfaces: (1) a mid-to-late Holocene shelf mud facies (present to *ca.* 7000 ^{14}C yr BP); (2) an early Holocene sand facies formed during transgression of sea level (*ca.* 10000 to 7000 ^{14}C yr BP); and (3) late Pleistocene coastal sand/mud deposits (*ca.* 25,000 to 11,000 ^{14}C yr BP) (Fig. 2). In particular, the lower sections of cores EZ2-20 and EZ4-10 containing well-developed sand and mud laminations are interpreted as deposits of a tide-influenced subtidal deltaic/estuarine environment during the sea-level lowstand when the paleo-shoreline was located 120 m below present-day sea-level (Saito et al., 1998; Kang et al., 2010).

Vertical variations of microfossil assemblages

We examined planktonic foraminiferal assemblages of core EZ02-20 sediments, spanning the *ca.* 20,000 ^{14}C yr BP. The foraminiferas were not identified in the lower sediment sections (<220 cm) because of its low occurrence (Table 2). In the samples, a total of 37 species were identified, all of which are commonly found in the modern northwestern Pacific Ocean and the ECS. The most abundant species with maximum percentages greater than 10% in at least one sample included *Globigerina bulloides*, *Globigerinita glutinata*, *Globigerinoides ruber*, *Neogloboquadrina dutertrei*, and *Pulleniatina obliquiloculata*. These five species account for more than 65% of the total planktonic foraminiferal assemblage in all subsamples of the core. *Globigerina falconensis*, *Globigerinoides sacculifer*, *Neogloboquadrina incompta*, and *Turborotalia crassaformis* also frequently occurred at maximum levels of less than 5%. The most common planktonic foraminifera in the upper section of the core (0–220 cm), which represents the mid-to-late Holocene deposits, was *G. bulloides* at 17.4–37% and showed an increased abundance until 90 cm, after which it exhibited gradual decline (Fig. 3b). *G. ruber*, *N. dutertrei*, and *P. obliquiloculata* vary in ranges of 8.2–22.4%, 9.7–20.4%, and 4.3–16.2%, respectively. The abundance, assemblage, and P/T ratio changed markedly at core depths of 220 cm, corresponding to *ca.* 7000 ^{14}C yr BP (Fig. 3a). The planktonic foraminifera in the sediments of lower section below 220 cm is low (<50 number g^{-1}) in occurrence, but it largely increases up to *ca.* 7500 number g^{-1} in the upper section. The P/T ratio gradually increased from an average of 19% below 220 cm to 42% above 200 cm. These results show an apparent paleoenvironmental change in the northern ECS shelf associated with a global sea level change during the late Pleistocene, involving a termination of the coastal water stage over the shelf at approximately 7000 ^{14}C yr BP when the warm KC began to flow into the ECS. The intrusion of warm Kuroshio waters at 8000–7000 ^{14}C yr BP is also recorded in several cores taken from marginal seas of the northwestern Pacific (Liu et al., 1992; Sawada and Handa, 1998; Kawahata et al., 2003; Kong et al., 2006).

Table 2
Species composition and relative percentage (%) of planktonic foraminifera in the core EZ02-20 from the northern East China Sea.

Species/depth (cm)	0	10	15	20	25	30	35	40	45	50	60	70	80	90	100	120	140	200	220	360	380	400	420	440	480
Beella digitata														0.5				0.5							
Globogerina angustiumbilicata			1.3				0.7	0.4		0.4	0.4		0.4		0.5				2.2		5.0	7.1		12.5	
Globigerina bulloides	30.0	30.7	28.3	21.6	37.2	29.1	31.8	27.7	36.3	21.5	23.8	21.9	25.6	34.5	35.5	25.7	25.4	20.9	17.4	100.0	15.0	28.6	15.4	25.0	
Globigerina calida					0.9	0.5			0.9	0.4	0.4		0.4				0.8								
Globigerina falconensis	4.2	4.7	3.0	2.6	3.7	3.6	5.2	3.5	3.8	3.6	4.3	3.3	2.9	1.8	4.1	3.7	4.7	1.5	2.2						
Globigerina foliata																0.5	2.1	1.0	4.3						
Globogerina quinqueloba	0.7	2.3	1.3		0.6	1.5	1.0	2.2	0.4	1.1	0.7	1.0		0.9	0.9	0.5	1.3	0.5			25.0	7.1			
Globigerina rubescens	0.7	0.9	2.1	1.9		1.0	1.0	3.0	0.9	2.2	2.1	0.5	0.8	1.4	1.4	0.9	2.5	2.0			5.0				
Globigerinella aequilateralis	2.1	0.5	0.4	3.9	0.9	1.0	1.4	1.7		1.5	0.4	1.4	1.2	0.9		1.8	0.4	1.0	2.2						
Globigerinita glutinata	8.1	5.1	8.0	4.2	7.0	10.7	7.3	9.1	9.8	8.4	6.4	7.1	7.4	7.7	14.5	9.2	8.5	8.7	15.2		5.0	14.3	7.7	25.0	
Globigerinita parkerae															0.5										
Globigerinita uvula			0.4								0.4		0.8				0.4								
Globogerinoides conglobatus	0.7	0.0		3.2	0.9	1.0	0.3		0.9	1.1	1.1	1.0	1.2	0.9	0.5	0.9	0.8	3.1	4.3						
Globigerinoides immaturus		1.4						0.9			0.4		0.4		0.5	1.8	3.0	2.0	2.2						
Globigerinoides quadrilobatus	2.8	2.8	0.4	2.9	0.3	1.0	1.0	1.3	1.7	1.8	1.8	3.3	2.1	1.8	0.9		0.4	1.0							
Globigerinoides ruber	17.0	14.9	22.4	18.4	17.4	18.9	15.2	13.0	15.0	17.5	19.5	16.2	13.2	10.5	8.2	18.3	13.1	12.8	10.9		15.0	7.1	15.4	25.0	
Globigerinoides pyramidalis	0.4																0.4								
Globigerinoides sacculifer	1.8	1.4	3.0	4.2	2.1	3.6	2.8	2.2	3.4	2.2	1.8			2.7	0.9	1.4		0.5	2.2						
Globigerinoides tenellus			0.4				0.7			0.4		1.4		0.9		0.5	0.8	1.0					7.7		
Globigerinoides	0.4																								
Globorotalia menardii		0.5	0.4	1.0		0.5	1.0	0.4	0.9	0.7	0.4					0.9									
Globorotalia obesa		0.9	0.4			1.0	0.3	0.4		0.4	0.4	0.5		0.5											
Globorotalia truncatulinoides		0.5																							
Globorotalia ungulata	0.4					0.5	0.3	0.4		0.7	1.4	0.5	1.7		0.5	0.5		1.5			5.0	7.1			
Globorotalia												0.5													
Globorotaloides hexagona																		0.5							
Hastigerina pelagica		0.5														0.9									
Neogloboquadrina dutertrei	12.7	12.6	9.7	16.1	10.1	13.3	9.7	13.4	11.1	20.4	18.4	15.7	16.5	15.9	15.5	11.5	14.0	16.8	17.4		15.0	28.6	23.1		
Neogloboquadrina incompta	1.8	6.0	5.1	1.3	6.4	4.1	3.5	3.9	6.0	4.4	2.8	5.7	4.5	4.5	6.4	6.0	6.4	4.6	4.3		10.0		15.4		
Neogloboquadrina pachyderma (s)			1.3		0.3		3.1																		
Neogloboquadrina pachyderma (d)	2.8	0.5	0.8		1.8	0.5	1.0	0.9	2.6	2.5	1.1	1.9	2.5	3.2	1.4	0.9	1.7	2.0	2.2					12.5	
Orbulina universa	0.4		0.4	0.6	0.3			0.9	0.4			0.5	0.8		0.5										
Pulleniatina obliquiloculata	10.6	12.1	9.7	13.5	8.5	7.1	9.3	8.7	4.3	6.9	9.9	16.2	16.1	10.9	7.3	9.6	5.1	8.2	13.0				7.7		100.0
Pulleniatina sp. A											0.7					1.8	1.3	4.6							
Turborotalia crassaformis	2.5	1.9	1.3	4.5	1.5	1.0	2.4	6.1	1.7	1.5	1.8	1.4	1.2	0.5	0.5	0.9	1.3								
Turborotalia inflata							0.3			0.7							0.4	1.5					7.7		
Turborotalita humilis							0.3																		
Miscellaneous (fragmented specimens)																1.8	5.1	3.6							
Total number of planktonic forams	283	215	237	310	328	196	289	231	210	275	282	210	242	220	220	218	236	196	46	1	20	14	13	8	1

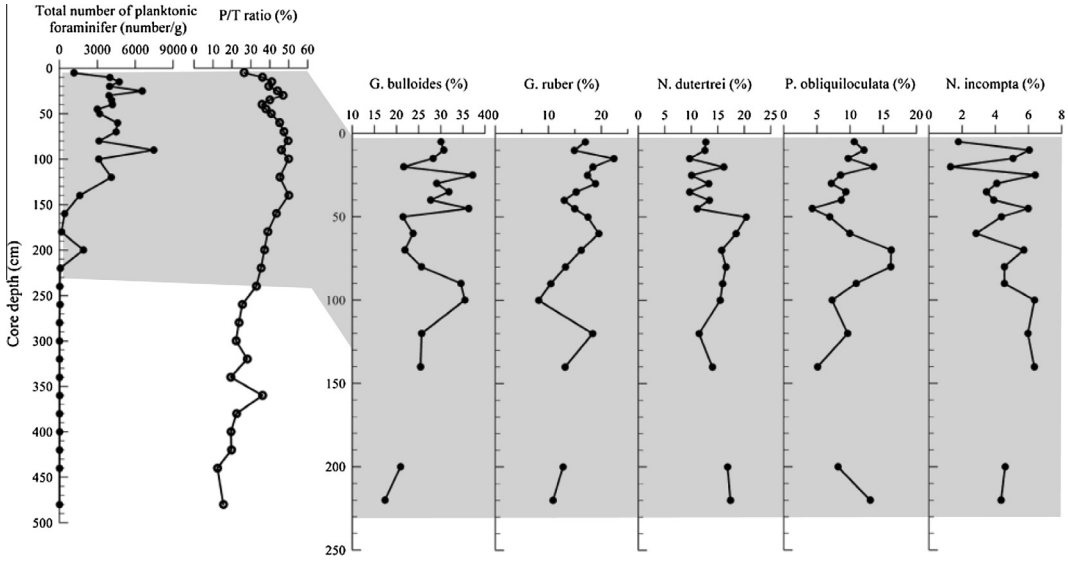

Fig. 3. Down-core variations in total number of planktonic foraminiferal, relative abundance of some major species and P/T ratio in core EZ2-20.

In total, 14 genera and 24 dinoflagellate cyst taxa were identified from cores EZ3-10 and EZ4-10 (Table 3). Cyst concentrations ranged between 1000 and 6000 number g^{-1}, except for core depths below 400 cm (<200 cysts g^{-1}). In core EZ2-20, the dominant species were *Spiniferites bulloideus* (23–64%), *Spiniferites* spp. (12–47%), *Operculodinium centrocarpum* (0–10%), *Spiniferites delicatus* (0–10%), *Nematosphaeropsis labyrinthus* (0–26%), and *Tuberculodinium vancampoae* (0–10%) (Fig. 4). Similarly, in core EZ4-10 the dominant species included *Spiniferites bulloideus* (0–67%), *Spiniferites* spp. (0–40%), *Brigantedinium* spp. (0–50%), *Spiniferites mirabilis* (0–14%), *Operculodinium centrocarpum* (0–25%), and *Spiniferites delicatus* (0–12%) (Fig. 4). In core EZ4-10, dinoflagellate cysts were rarely observed or absent in the late Pleistocene deltaic/estuarine sediments. In contrast, dinoflagellate cyst concentrations showed an increase in the upper core sections, indicating a major transition from a deltaic/estuarine environment to a full-oceanic environment suitable for colonization by dinoflagellates. The dinoflagellate cyst assemblages of the Holocene deposits were characterized by a predominance of the gonyaulacoid group (e.g., genera *Spiniferites*, *N. labyrinthus*, *O. centrocarpum*, and *Lingulodinium machaerophorum*), which constituted *ca.* 83–99% and 79–94% of total cyst concentrations in cores EZ3-10 and EZ4-10, respectively (Fig. 5). Such notable increase in the gonyaulacoid species indicates increased nutrient loadings in the upper water column of the northern ECS since the onset of the early Holocene (Kim et al., 2012).

Discussion

Signatures of the late Holocene cold event in the ECS shelf

Sedimentological and micropaleontological records of the core sediments from the study area show that there was a major environmental change from a pre-Holocene deltaic/estuarine environment to a full-oceanic environment of the mid-to-late Holocene in the northern ECS shelf (Fig. 2). The evidence presented here suggests that the present-day oceanographic conditions were established over the shelf region at around 7000 ^{14}C yr BP. Coinciding with the flooding of the estuarine shelf, significantly improved marine productivity is indicated by a notable increase of planktonic foraminifera and dinoflagellate cysts in Holocene deposits (Figs. 3 and 5). Such improvement of marine productivity may be primarily caused by the post-glacial sea-level rise which resulted in an expansion of marine habitats suitable for micro-organisms. Additionally, we suggest that the increase of the micro-organism community in the shelf water can be attributed, at least in part, to enhanced nutrient supply by palaeo-river discharge from the adjacent continent. The suggested postglacial nutrient enrichment corresponds in time with the Holocene climatic optimum that developed at 10,000–7500 ^{14}C yr BP and terminated at 5000–2000 ^{14}C yr BP (An et al., 2000; An et al., 2006). Considering that the Holocene climatic optimum is regarded as the time of maximum precipitation in central and eastern China (e.g., Bates and Jackson, 1987; Shi et al., 1993), increased moisture availability over the Chinese continent would have resulted in a massive river discharge and thus an increased nutrient supply to the northern ECS region. In the late Holocene, however, the postglacial marine productivity increase appears to be punctuated, notably at between 4000 and 2500 ^{14}C yr BP (Fig. 5). A recently published dinoflagellate cyst record from this area demonstrated that the lower concentration of dinoflagellate cysts during this period indicates a deterioration of nutrient availability (Kim et al., 2012). Similar trends can be observed in a previous dinoflagellate cyst investigation on the northern ECS shelf sediments (Cho, 2000), where an interval of low dinoflagellate cyst concentrations (core ST-11; location indicated in Fig. 1) points to the late Holocene period (Fig. 5). We, therefore, suggest that the late Holocene reduction in dinoflagellate cysts, coherently observed in the three core records, reflects a deterioration of nutrient availability in the northern ECS shelf environment.

Furthermore, the late Holocene deterioration of oceanic condition, in terms of sea-surface temperatures (SSTs), is clearly implicated in variations of the planktonic foraminiferal assemblage of core EZ2-20. On the basis of previous studies that analyzed relationships between occurrence of recent planktonic foraminifera assemblages and oceanographic conditions in the northwestern Pacific, the equatorial Pacific, and the ECS, planktonic foraminifers can be classified into four groups (Bé, 1977; Thompson, 1981; Wang et al., 1985; Li et al., 1997; Xu and Oda, 1999; Ujiié and Ujiié, 1999; Ujiié et al., 2003; Ijiri et al., 2005; Lim et al., 2006): tropical-subtropical assemblage (Group A), Kuroshio assemblage (Group B), cold assemblage (Group C), and coastal water assemblage with low salinity and/or low temperature (Group D) (Table 4). As shown in vertical profiles of planktonic foraminieral assemblage in the core EZ02-20 (Fig. 6), a prominent decline in the tropical-subtropical

Table 3
Species composition and abundance (cysts per gram) of dinoflagellate cysts in cores EZ3-10 and EZ04–10 from the northern East China Sea.

Species/depth (cm)	5	10	20	30	40	50	60	70	80	90	100	110	120	130	140	150	160	170	180	190	200	210	220	230	240	250	260	270	280	290	300	310	320	330	340	350	360
Gonyaulacoid group																																					
Nematosphaeropsis labyrinthus	329	66	55	173	24	118	0	68	835	81	35	65	320	496	194	61	77	11	48	453	111	224	35	29	81	45	69	100	109	63	8	128	8	60	118	21	117
Lingulodinium machaerophorum	6	19	0	14	24	0	10	0	79	16	17	11	0	25	0	12	13	11	10	4	18	11	17	0	0	18	0	19	0	38	0	0	0	12	0	0	0
Spiniferites bentorii	11	19	18	43	47	0	69	15	32	0	26	33	20	50	43	61	0	22	48	22	55	11	17	14	0	45	28	13	39	0	0	0	0	6	17	0	16
Spiniferites bulloideus	698	1088	893	1240	1544	1936	1512	942	898	1457	1416	2373	2218	4613	2797	2875	1929	3053	2532	2873	2274	2093	1249	1629	1364	1729	1606	1381	1431	428	902	922	1337	883	465	970	749
Spiniferites delicatus	195	38	120	115	204	43	227	98	173	16	79	163	60	422	65	195	64	66	68	435	37	139	35	0	97	323	42	151	178	138	157	43	128	138	101	52	31
Spiniferites hyperacanthus	33	19	37	29	133	96	69	45	32	81	44	293	100	446	32	97	26	110	19	67	92	43	26	43	32	125	69	100	79	0	41	34	40	12	42	21	0
Spiniferites membranaceus	6	0	9	0	31	0	0	0	0	0	0	22	0	0	11	24	0	0	0	13	0	0	0	0	16	9	0	13	10	0	0	0	0	0	8	0	0
Spiniferites mirabilis	56	47	18	115	47	107	89	90	63	130	52	130	120	124	86	122	39	55	39	94	111	43	52	72	65	81	194	44	59	38	8	102	40	66	17	41	62
Spiniferites ramosus	73	47	28	43	16	139	69	23	221	81	44	217	60	0	32	24	13	44	48	54	148	11	17	43	32	54	14	44	20	0	8	51	8	12	8	41	8
Spiniferites spp.	352	747	497	1182	384	1562	474	1175	378	1376	682	1365	899	2183	925	816	977	1113	1247	1136	1137	748	515	721	1218	564	789	684	1086	893	505	461	408	378	600	413	725
Operculodinium centrocarpum	128	104	111	159	180	96	296	105	268	178	184	184	260	0	151	219	51	121	145	189	176	43	122	130	162	287	111	301	227	88	166	111	128	78	93	103	148
Impagidinium spp.	0	0	0	0	0	21	0	8	0	16	0	0	0	0	22	0	0	0	0	13	0	0	0	0	0	0	0	0	10	0	0	9	0	12	0	0	0
Gymnodinioid group																																					
Polykrikos kofoidii	17	9	0	14	0	11	20	0	0	16	0	11	0	0	22	12	0	55	39	36	28	11	26	14	0	45	0	0	0	0	25	9	0	6	0	10	0
Polykrikos schwartzii	6	0	0	0	0	0	0	0	0	0	9	0	0	50	11	0	0	0	0	4	0	0	0	29	32	0	0	0	0	13	0	0	0	6	0	0	8
Tuberculodinioid group																																					
Tuberculodinium vancampoae	61	47	46	72	63	182	119	121	142	113	105	33	20	0	118	97	129	55	58	49	55	43	70	43	32	125	97	119	168	126	149	111	128	72	93	93	226
Protoperidinioid group																																					
Brigantedinium spp.	73	19	28	72	16	32	20	8	32	97	17	22	60	99	22	49	116	22	39	81	55	85	9	14	0	18	28	19	30	0	25	94	32	18	42	10	101
Quinquecuspis concretum	0	0	9	0	0	0	10	0	0	0	0	0	0	0	0	0	0	0	0	4	0	0	0	0	0	0	0	0	0	0	0	0	0	0	0	0	0
Stelladinium spp.	0	0	9	14	0	0	10	0	0	0	0	11	0	0	0	24	0	22	0	4	0	11	0	0	0	0	14	13	10	0	0	9	8	0	0	21	0
Selenopemphix nephroides	6	0	0	0	0	21	0	0	0	0	0	0	0	0	0	0	0	0	0	0	0	0	0	14	0	0	28	0	0	0	0	26	8	12	17	0	8
Selenopemphix quanta	0	28	0	0	16	0	10	15	0	16	35	0	0	50	22	12	13	11	29	9	28	53	0	0	16	0	0	13	20	63	0	17	0	12	17	21	31
Trinovantedinium applanatum	0	38	0	0	0	0	0	0	47	0	17	0	0	0	11	0	13	11	0	18	0	11	9	0	0	9	0	0	10	13	33	17	8	6	8	10	0
Votadinium calvum	6	0	0	0	0	0	0	0	0	16	0	0	0	0	0	0	0	0	0	0	0	0	0	0	0	0	0	0	0	0	0	0	0	0	0	0	0
Xandarodinium xanthum	0	0	0	0	0	0	0	15	0	0	0	0	0	0	11	0	0	0	0	0	0	0	0	0	0	0	0	0	0	0	0	0	0	0	0	0	0
Total cysts per gram	2054	2336	1879	3287	2728	4364	3004	2728	3198	3691	2762	4930	4136	8557	4571	4702	3460	4783	4369	5562	4326	3578	2202	2797	3151	3476	3088	3013	3484	1899	2028	2144	2281	1790	1648	1826	2230

Species/depth (cm)	5	20	40	60	80	100	120	140	160	180	200	220	240	260	280	300	320	340	360	380	400	420	440	460	480	500	520	540
Gonyaulacoid group																												
Nematosphaeropsis labyrinthus	34	2	4	0	53	0	43	25	30	0	47	76	108	27	8	118	42	11	455	14	22	0	0	9	0	0	0	0
Lingulodinium machaerophorum	13	2	0	5	13	7	14	25	0	14	8	4	10	9	0	31	49	23	6	10	17	0	20	66	5	5	0	4
Spiniferites bentorii	25	4	14	5	18	13	43	49	10	62	71	54	59	90	84	55	76	23	18	14	77	0	60	236	15	0	0	0
Spiniferites bulloideus	488	249	466	615	454	747	555	1353	307	777	1318	1091	665	566	870	675	506	467	748	242	28	6	7	47	0	0	0	0
Spiniferites delicatus	110	32	42	45	94	168	151	386	37	179	298	284	283	162	186	228	76	56	180	48	11	0	0	28	0	0	0	0
Spiniferites hyperacanthus	0	4	21	5	27	0	86	0	0	34	71	101	225	63	51	55	35	6	0	3	22	0	40	38	0	0	0	0
Spiniferites membranaceus	0	0	0	0	4	0	7	0	0	7	31	36	29	18	25	39	0	0	18	0	0	0	0	0	0	0	0	0
Spiniferites mirabilis	119	38	49	121	94	249	202	517	67	76	361	331	401	198	253	110	62	39	18	45	22	0	33	9	5	5	0	4
Spiniferites ramosus	42	26	28	40	85	81	29	246	13	55	157	148	108	99	59	118	76	6	54	24	6	0	0	38	0	0	0	0
Spiniferites spp.	233	158	288	328	717	390	584	582	135	158	502	464	450	315	211	173	166	304	311	169	94	3	53	47	5	0	0	21
Operculodinium centrocarpum	140	32	39	60	67	175	94	328	61	89	173	173	254	171	144	110	104	107	78	31	17	0	20	47	20	16	0	4
Operculodinium israelianum	4	0	4	20	0	7	7	16	3	0	0	0	0	0	0	0	0	0	0	0	0	0	0	0	0	0	0	0
Impagidinium spp.	0	2	4	0	0	7	0	0	0	0	0	0	0	0	0	0	0	6	0	0	0	0	0	0	0	0	0	0
Gonyaulacoid group %	79	87	84	91	91	93	85	94	88	92	93	92	90	91	86	87	92	81	91	91	73	100	56	73	48	42	0	35
Gymnodinioid group																												
Polykrikos kofoidii	8	4	7	15	0	0	29	0	20	62	0	25	20	9	34	94	0	45	12	10	11	0	0	19	0	0	0	0
Polykrikos schwartzii	42	0	0	0	0	0	7	8	0	0	0	0	0	9	0	8	7	0	0	0	0	0	0	0	0	0	0	0
Gymnodinioid group %	3	1	1	1	0	0	2	0	3	4	0	1	1	1	2	5	1	3	1	2	3	0	0	2	0	0	0	0
Tuberculodinioid group																												
Tuberculodinium vancampoae	47	2	56	40	31	54	180	107	27	41	86	90	117	27	194	110	42	45	90	24	11	0	33	57	0	5	0	13
Tuberculodinioid group %	3	0	5	3	2	3	8	3	4	3	3	3	4	1	9	6	3	3	4	4	3	0	8	7	0	8	0	13
Protoperidinioid group																												
Brigantedinium spp.	212	64	98	66	94	61	58	82	37	21	118	108	59	54	51	24	28	113	54	21	88	0	140	113	30	33	0	34
Quinquecuspis concretum	0	6	0	0	0	0	0	0	0	0	0	0	0	9	8	0	0	0	6	0	6	0	0	0	0	0	0	0
Stelladinium bifurcatum	0	0	4	0	9	7	0	0	0	0	0	0	0	0	0	16	0	0	0	0	0	0	0	0	0	0	0	0
Selenopemphix nephroides	4	0	4	5	4	0	7	0	0	0	16	11	10	0	0	8	0	6	0	0	0	0	7	0	0	0	0	0
Selenopemphix quanta	8	4	0	0	4	7	22	0	10	0	8	11	20	27	17	0	28	28	18	7	0	0	0	19	25	0	0	17
Trinovantedinium capitatum	4	2	14	0	13	7	0	16	0	0	0	0	10	0	0	8	0	11	12	0	0	0	0	0	0	0	0	0
Votadinium calvum	4	0	0	0	0	0	0	0	0	0	8	4	0	0	0	0	0	0	6	0	0	0	0	0	0	0	0	0
Xandarodinium xanthum	0	0	0	0	4	0	7	0	0	7	8	4	39	36	8	0	0	0	0	0	0	0	0	0	0	0	0	0
Protoperidinioid group %	15	12	10	5	7	4	4	3	6	2	5	5	5	7	4	3	4	12	5	4	22	0	35	17	52	50	0	52
Total cysts per gram	1540	633	1140	1371	1786	1979	2126	3740	758	1581	3280	3013	2864	1887	2204	1979	1297	1295	2082	662	431	10	413	775	104	66	0	99

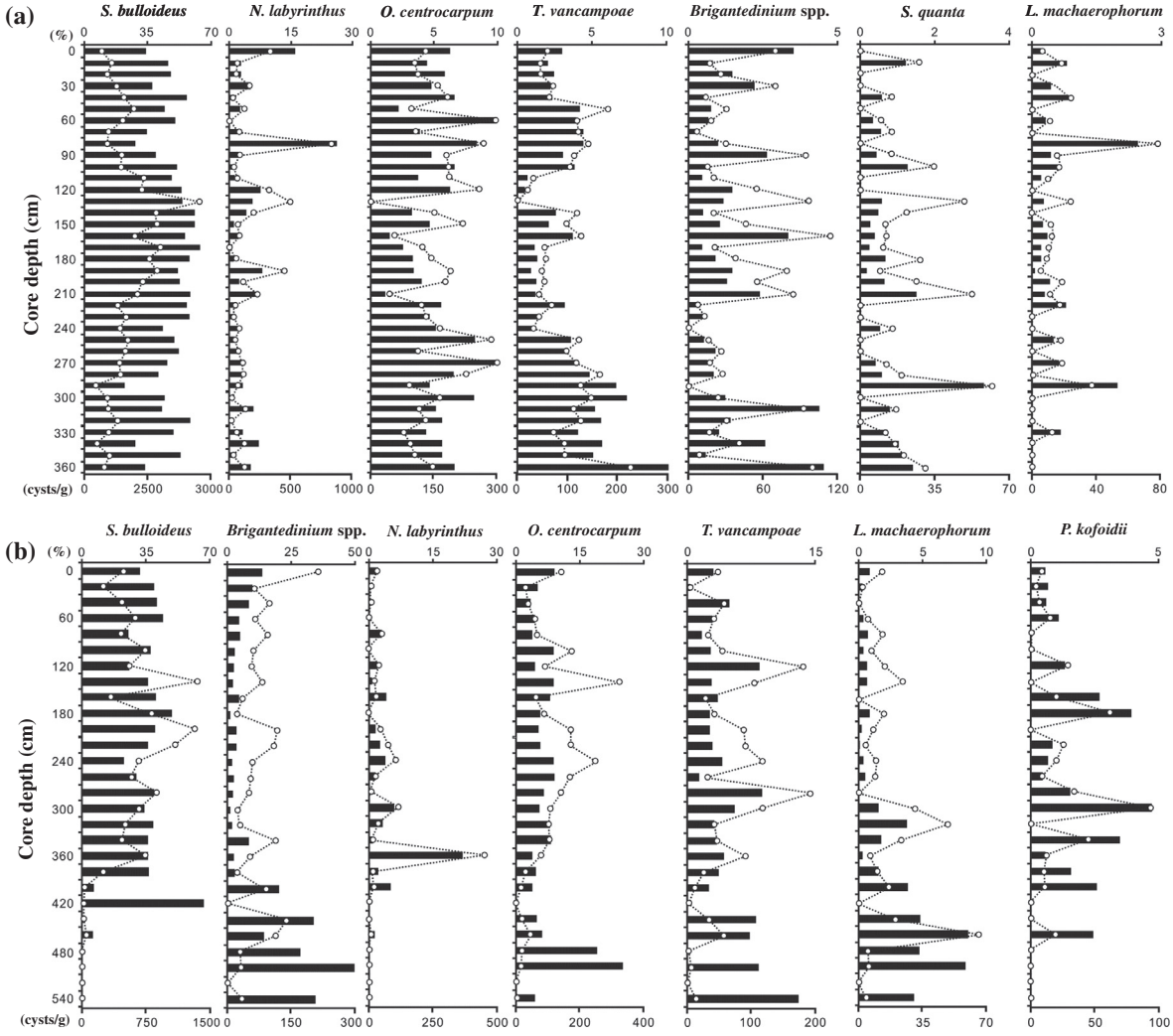

Fig. 4. Total numbers (black bar) and relative abundance (open circle) of major dinoflagellate cysts from cores EZ3-10 (a) and EZ4-10 (b).

species and the warm Kuroshio water species together with a marked increase in cold and coastal water species at 4500–2500 ^{14}C yr BP clearly point to reduced SSTs and sea-surface salinity (SSS) as a result of a weakened influence of the warm KC waters on the northern ECS. Taken together, the synchronous changes between dinoflagellate cyst and planktonic foraminiferal assemblages during the late Holocene point to a major environmental shift in nutrient availability as well as SSTs, linked to a weakened KC influence over the northern ECS shelf and the termination of the Holocene climatic optimum.

A global perspective on the late Holocene Neoglacial events

The late Holocene climatic events of the cores in this study show good correspondence with other marine records from the northwestern Pacific margin. The reduced nutrient availability and surface-water productivity during the late Holocene period have been reported from the Ulleung Basin of the East Sea, where the carbonate content of the sediments showed an abrupt decrease during the period 3600–2500 ^{14}C yr BP (Lim et al., 2011). In the middle Okinawa Trough in the South China Sea (SCS) (Xiang et al., 2007), the Holocene sediments are generally dominated by warm water species such as *G. ruber*, *G. sacculifer*, *G. glutinata*, and *P. obliquiloculata* (A7 and E017 cores; sampling sites are indicated in Fig. 1). However, for the period between 4600 and 2300 cal yr BP, a remarkable decrease in the Kuroshio water species *P. obliquiloculata* and an increase in the coastal water species *G. bulloides* were recorded (Fig. 7). Similar records of the so-called *Pulleniatina* minimum event have been found in previous studies (e.g., Ujiié and Ujiié, 1999; Ijiri et al., 2005; Jian et al., 2000). In Lee et al. (2010), summer and winter SSTs of core sediments from the southeastern part of the Ulleung Basin in the East Sea register a notably lower value at around 3000 cal yr BP. Such low SSTs in East Sea are also indicated by the decrease of *Fragilariopsis doliolus* and the diatom-estimated temperature (Koizumi et al., 2006). Consequently, these coherent late Holocene climatic events recorded in the northwestern Pacific marginal seas (i.e., East Sea, SCS, and ECS) suggest a cooling of surface waters in association with a sudden decrease in the warm Kuroshio water influence.

The Kuroshio water originates from subtropical and tropical regions with low nutrient contents near the surface (Chen, 1996). Therefore, the decreased marine primary productivity during this time period would not be directly affected by fluctuations of the Kuroshio water input itself. Several studies suggested that freshwater discharges from large rivers (e.g., Changjiang) in the adjacent continent are a main source of nutrient input to the ECS region (Beardsley et al., 1985; Chang et al., 2003). Therefore, we speculate that the deterioration of primary marine productivity superimposed on the SST cooling trend in the northern ECS shelf are attributable to an abrupt change in moisture contents over the adjacent

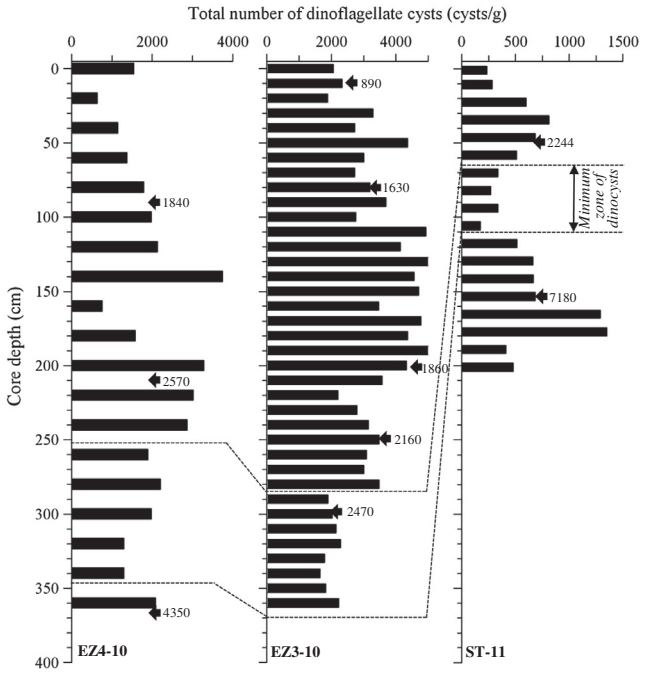

Fig. 5. Correlation in vertical variations of total dinoflagellate cyst concentrations in cores EZ3-10, EZ4-10 and ST-11. Numbers with arrows are radiocarbon ages (^{14}C yr BP).

Table 4
Four faunal groups of planktonic foraminifera based on modern planktonic assemblages of the Pacific marginal seas (after Lim et al. 2006).

Species	Water mass
Assemblage A	
Globigerinoides ruder group (*G. ruder* + *G. pyramidalis*)	Tropical-subtropical water
Globigerinoides conglobatus	
Globigerinoides sacculifer	
Globigerinoides cf. *sacculifer*	
Globigerinoides tens	
Globigerinoides aequilateralis	
Assemblage B	
Globorotalia menardii	Kuroshio water
Neogloboquadrina dutertrei	
Pulleniatina obliquiloculata	
Assemblage C	
Globorotalia truncatulinoides	Cold water
Neogloboquadrina incompta	
Neogloboquadrina Pachyderma(s)	
Neogloboquadrina Pachyderma(d)	
Turborotalia inflate group (*T. inflate* + *T. crassaformis*)	
Assemblage D	
Globigerina bulliodes	Coastal water (low salinity and/or low temperature)
Globigerina calida	
Globigerina quinqueloba	

continent, which in turn controls nutrient supplies into the surface waters. This interpretation is supported by previous work on terrestrial records from northern China. According to Jin et al. (2004), climate proxy data from the Daihai Lake in northern China show that Holocene climate oscillations, including the Hypsithermal and the Neoglaciation, were punctuated by several decadal- to millennial-scale changes from warm to cool and/or wetter to drier conditions (Fig. 7). Sediment records from the Daihai Lake suggest that the warm and humid Hypsithermal period was resulted in a significant enhancement of terrestrial chemical weathering and a gradual increase in terrestrial plants. This suggestion is also supported by other high lake level records between ~9000 and 4000 years ago (Zhang, 1937; Wang and Li, 1990; Wang et al., 1990). After the end of the Hypsithermal warming interval (*ca.* ~3500 to 4000 years ago), the lake sediment records indicated limited terrestrial plant growth in semi-arid and semi-humid regions of northern China implying lowered temperatures and reduced weathering. A similar trend of terrestrial cooling linked to growing aridity have also been reported from other parts of the East Asian continent including Korean peninsula (e.g. Chung, 2011 and references therein). The climate transition from warmer/wetter to cooler/drier conditions in the northern Asia during the late Holocene coincides with Holocene fluctuations of mountain glaciers on the Tibetan Plateau. During the Early Holocene (10,000–7500 years ago), high lake levels and peat development in the Tibetan Plateau and surrounding areas indicate relatively wet and warm paleoclimatic conditions. These conditions were followed by the Holocene climatic optimum (7500–3000 years ago), which features warmer conditions than the present day (Gasse et al., 1991; Holland et al., 1991; Wang and Fan, 1987; Beug, 1987; Wang, 1987). Later, a negative trend occurred during the late Holocene. The cooling episode of the late Holocene is characterized by glacial advances over much of the Tibetan Plateau (Lehmkuhl, 1997; Fig. 7). In conclusion, the late Holocene terrestrial climatic transition in northern China appears to be synchronous with the oceanic environmental shift in the northern ECS shelf, reflected in our microfossil records. This finding suggests a close linkage between marine and terrestrial processes in past climatic changes in the northwestern Pacific margin. Given that SST variations in monsoonal regions have a crucial role in modulating land-sea heating and pressure gradients, and thus directly affecting the intensity of precipitation and runoff patterns over the adjacent continent (e.g., Schefuß et al., 2003; Weldeab et al., 2005), a possible explanation for the enhanced aridity over northern China during the late Holocene period involves SST cooling events associated with the weakened KC. In parallel, the shift in these late Holocene marine and terrestrial records of the northwestern Pacific margin is coeval with records of climatic variations observed in northern high latitude regions. The so-called Neoglacial (or Neoglaciation) interval that began in the mid-Holocene and lasted more than 2000 years has been characterized by a marked sea-ice expansion over the East Greenland shelf (Jennings et al., 2002) and the western Arctic Ocean such as Chukchi Sea shelf (de Vernal et al., 2005) and the Canada Basin (Farmer et al., 2011), coastal glacier expansions over the Gulf of Alaska (Calkin et al., 2001), intensely erosive storms along the Chukchi Sea coast (Mason and Barber, 2003) and pronounced cooling events in the western Bering Sea (Razjigaeva et al., 2004). This trend supports the notion that climatic events of the northern Pacific Ocean are closely linked to the global climate system through hydrological dynamics in the Pacific sector of the Arctic Ocean (Woodgate et al., 2007, 2010; Hu et al., 2010, 2012).

In the northwest Pacific marginal seas, the weakened KC and reduced SSTs during the late Holocene have often been linked to an intensified winter monsoon and strengthened coastal currents (Li et al., 1997; Jian et al., 2000). However, it has recently become clear that the Holocene climatic fluctuations recorded in the ESC and SCS are closely linked to the path and strength of the KC in the East Asian marginal seas (Ijiri et al., 2005; Xiang et al., 2007; Chang et al., 2008). Therefore, we speculate that the suggested integration of both marine and terrestrial signals in the northwestern Pacific margin during the late Holocene could be related to global, not only regional climatic processes. In particular, the synchronicity of the late Holocene climatic events between the middle latitude northwestern Pacific margin and the northern high-latitude region

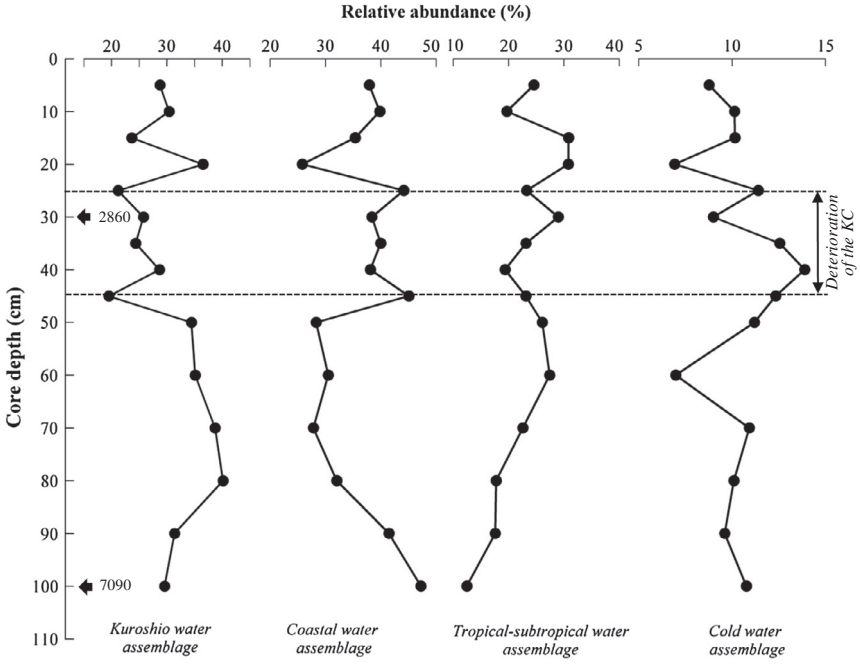

Fig. 6. Down-core variation in the relative abundances of four planktonic foraminifer assemblages during the mid-to-late Holocene periods. Note that the abrupt change in their assemblage between 25 and 45 cm, corresponding to approximately 3500–2800 years BP. Numbers indicate the radiocarbon ages (^{14}C yr BP).

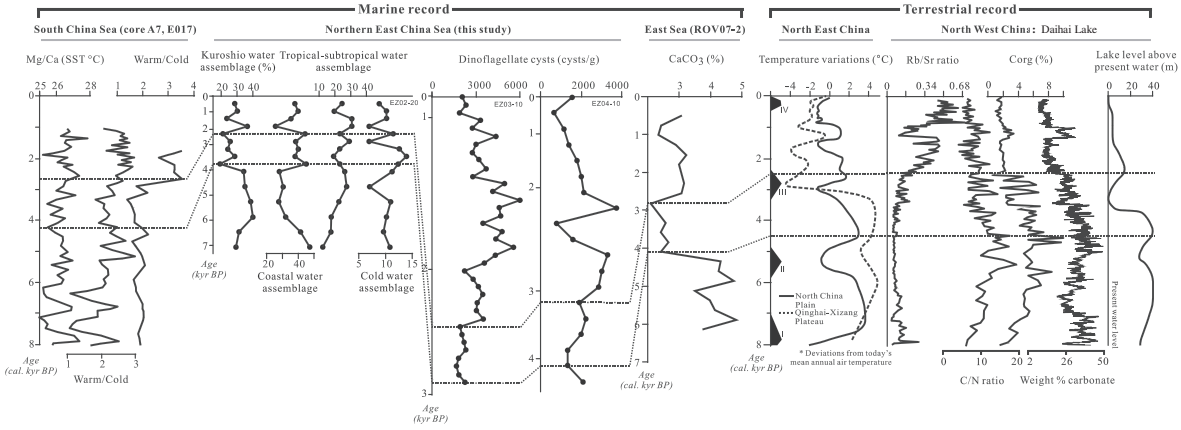

Fig. 7. Integrated marine–terrestrial proxy records in the northwestern Pacific margin for the late Holocene period. Terrestrial records from: temperature variations in the North East China (after Lehmkuhl, 1997), Rb/Sr ratio, C/N ratio, C_{org}, weight percent carbonate and lake level in the North West China (after Jin et al., 2004). The interval of the late Holocene climatic event is indicated by dotted lines.

highlights a role of the global ocean circulation system, which regulates dynamics of the North Pacific gyre and the high-latitude North Atlantic thermohaline circulation, and therefore the mean latitude of the Kuroshio extension (Sawada and Handa, 1998; Isono et al., 2009). This notion is supported by recently published statistical analysis of a global set of Holocene time series from palaeoclimate archives (Wanner et al., 2011), in which the cooling event between 3300 and 2500 yr BP was hypothetically explained by fluctuations of the thermohaline circulation, as well as interconnected dynamics between the North Atlantic and Pacific regions.

Conclusions

Records of microfossil assemblages, including dinoflagellate cysts and planktonic foraminifers, in three piston cores from the northern shelf of the ECS indicate a marked change in paleo-depositional environments in the northern ECS since the LGM from a deltaic/estuarine environment to a fully-oceanic environment. A rapid increase in dinoflagellate cysts and planktonic foraminifera during the early to mid-Holocene interval points to optimized climatic conditions in terms of SSTs and nutrient availability. In contrast to the warm and wet Holocene climatic optimum period, the late Holocene interval, particularly between 4000 and 2500 ^{14}C yr BP, registers a remarkable decrease in dinoflagellate cysts and a sudden increase in cold-water planktonic foraminiferal species, suggesting a weakened KC influence. The correlation between the deteriorated oceanic condition and terrestrial cooling and dry episodes in northern China highlights a significance of atmosphere–ocean dynamics regulating moisture and heat distribution over the northwestern Pacific margin. The late Holocene ocean-land climate fluctuations in the northwestern Pacific are synchronous to the Neoglacial events recorded in areas farther to the north. This might imply that the particular event, superimposed on the late Holocene, was not localized to the northwestern Pacific margin and represents a global climate signal in which mechanisms

transferring climatic variability between different latitudes and systems are embedded. Our study also emphasizes an important role of the global ocean circulation system in the climatic synchronicity between different latitudes and systems. Further studies are needed to correlate existing records of pure marine or terrestrial sequences for better understanding on the links between the ocean-land processes at different timescales covering a wide latitudinal transect including a number of atmospheric, terrestrial, and marine systems with different sensitivity to climatic changes.

Acknowledgements

This study was supported by Korea Institute of Ocean Science and Technology (KIOST) research program (Grant no. PE99233), and also partly funded by the Korea Polar Research Institute research program (Grant No. PE14062 and PP13030). We thank "Library of Marine Samples (LIMS)" in KIOST for supplying the core sediments.

References

An, Z., Porter, S.C., Kutzbach, J.E., Wu, X., Wang, S., Liu, X., Li, X., Zhou, W., 2000. Asynchronous Holocene optimum of the East Asia monsoon. Quaternary Science Reviews 19, 743–762.

An, C.B., Feng, Z.D., Barton, L., 2006. Dry or humid? Mid-Holocene humidity changes in arid and semi-arid China. Quaternary Science Reviews 25, 351–361.

Bates, R.L., Jackson, J.A., 1987. Glossary of Geology. American Geological Institute, Alexandria, VA.

Bé, A.W.H., 1977. An ecological, zoo-geographical and taxonomic review of recent planktonic foraminifera. In: Ramsay, A.T.S. (Ed.), Ocean Micropaleontology 1. Academic, London, pp. 1–100.

Bé, A.W.H., Tolderlund, D.S., 1971. Distribution and ecology of living planktonic foraminifera in surface waters of the Atlantic and Indian Oceans. In: Funnel, B.M., Riedel, W.R. (Eds.), Micropaleontology of Oceans. Cambridge University Press, London, pp. 105–149.

Beardsley, R.C., Limeburner, R., Yu, H., Cannon, G.A., 1985. Discharge of the Changjiang (Yangtze River) into the East China Sea. Continental Shelf Research 4, 57–76.

Beug, H.J., 1987. Palynological Studies on a peat layer in Kakitu Mountain, Northeastern Qinghai-Xizang Plateau. In: Hövermann, J., Wenying, W. (Eds.), Reports of the Qinghai-Xizang (Tibet) Plateau. Beijing, pp. 496–501.

Bond, G., Showers, W., Cheseby, M., Lotti, R., Almasi, P., deMenocal, P., Priore, P., Cullen, H., Hajdas, I., Bonani, G., 1997. A pervasive millennial-scale cycle in North Atlantic Holocene and glacial climates. Science 278, 1257–1266.

Bond, G., Kromer, B., Beer, J., Muscheler, R., Evans, M.N., Showers, W., Hoffmann, S., Lotti-Bond, R., Hajdas, I., Bonani, G., 2001. Persistent solar influence on North Atlantic climate during the Holocene. Science 294, 2130–2136.

Calkin, P.E., Wiles, G.C., Barclay, D.J., 2001. Holocene coastal glaciation of Alaska. Quaternary Science Reviews 20, 449–461.

Chang, J., Shiah, F.K., Gong, G.C., Kuo, P.C., 2003. Cross-shelf variation in carbon-to-chlorophyll a ratios in the East China Sea, summer 1998. Deep-Sea Research II 50, 1237–1247.

Chang, Y.P., Wang, W.L., Yokoyama, Y., Matsuzaki, H., Kawahata, H., Chen, M.T., 2008. Millennial-Scale Planktic Foraminifer Faunal Variability in the East China Sea during the Past 40,000 Years (IMAGES MD012404 from the Okinawa Trough). Terrestrial Atmospheric and Oceanic Sciences 19 (4), 389–401.

Chen, C.T.A., 1996. The Kuroshio intermediate water is the major source of nutrients on the East China Sea continental shelf. Oceanologica Acta 19 (5), 523–527.

Cho, H.J., 2000. Utility of Dinoflagellates in Studying the Marine Environment: The Case of the East China Sea and Adjacent Areas. Ph.D. Thesis, Nagasaki University, Japan.

Cho, H.J., Matsuoka, K., 1999. Dinoflagellate cyst composition and distribution in the surface sediments from the Yellow Sea and the East China Sea. In: Proceedings of 2nd Workshop on Oceanography and Fisheries in the East China Sea "The East China Sea" vol. 2. Nagasaki University, Japan, pp. 73–81.

Chung, C.H., 2011. Holocene vegetation dynamics and its climatic implications inferred from pollen record in Boseong area, South Korea. Geosciences Journal 15 (3), 257–264.

deMenocal, P., Ortiz, J., Guilderson, T., Sarnthein, M., 2000. Coherent High- and Low-Latitude Climate Variability During the Holocene Warm Period. Science 288, 2198–2202.

de Vernal, A., Hillaire-Marcel, C., Darby, D.A., 2005. Variability of sea ice cover in the Chukchi Sea (western Arctic Ocean) during the Holocene. Paleoceanography 20, PA4018.

de Vernal, A., Marret, F., 2007. Organic-walled dinoflagellate cysts: tracers of sea-surface conditions. Developments in Marine Geology 1, 371–408.

Dykoski, C.A., Edwards, R.L., Cheng, H., Yuan, D., Cai, Y., Zhang, M., Lin, Y., Qing, J., An, Z., Revenaugh, J., 2005. A highresolution absolute-dated Holocene and deglacial Asian monsoon record from Dongge Cave, China. Earth and Planetary Science Letters 233, 71–86.

Farmer, J.R., Cronin, T.M., de Vernal, A., Dwyer, G.S., Keigwin, L.D., Thunell, R.C., 2011. Western Arctic Ocean temperature variability during the last 8000 years. Geophysical Research Letters 38, L24602.

Gasse, F., Arnold, M., Fontes, J.C., Fort, M., Gilbert, E., Huc, A., Li, B., Li, Y., Lui, Q., MElirres, F., VanCampo, E., Wang, F., Zhang, Q., 1991. A 13,000-Year climate record from western Tibet. Nature 353, 742–745.

Gupta, A.K., Sarkar, S., Mukherjee, B., 2006. Paleoceanographic changes during the past 1.9 Myr at DSDP Site 238, Central Indian Ocean Basin: Benthic foraminiferal proxies. Marine Micropaleontology 60, 157–166.

Hama, T., Shin, K.H., Handa, N., 1997. Spatial variability in the primary productivity in the East China Sea and its adjacent waters. Journal of Oceanography 53, 41–51.

Hemleben, C., Spindler, M., Anderson, O.R., 1998. Modem Planktonic Foraminifera. Springer, New York, pp. 1–363.

Holland, H.D., Smith, G.I., Jannasch, H.W., Dickson, A.G., Zheng, M., Ding, T., 1991. Lake Zabuye and the climate history of the Tibetan Plateau. die Geowissenschaften 9 (2), 37–44.

Hsueh, Y., 2000. The Kuroshio in the East China Sea. Journal of Marine System 24, 131–139.

Hu, A., Meehl, G.A., Otto-Bliesner, B.L., Waelbroeck, C., Han, W., Loutre, M.F., Lambeck, K., Mitrovica, J.X., Rosenbloom, N., 2010. Influence of Bering Strait flow and North Atlantic circulation on glacial sea-level changes. Nature Geosciences 3, 118–121.

Hu, A., Meehl, G.A., Han, W., Timmermann, A., Otto-Bliesner, B., Liu, Z., Washington, W.M., Large, W., Abe-Ouchi, A., Kimoto, M., Lambeck, K., Wu, B., 2012. Role of the Bering Strait on the hysteresis of the ocean conveyor belt circulation and glacial climate stability. PNAS 24 (109/17), 6417–6422.

Hyun, S.M., Lim, D.I., Yoo, H.S., 2006. Transgressive geochemical records in the East China Sea: a perspective with Holocene paleoceanography. Economical and Environmental Geology 39, 53–61.

Ichikawa, H., Chaen, M., 2000. Seasonal variation of the heat and freshwater transports by the Kuroshio in the East China Sea. Journal of Marine System 24, 119–129.

Ijiri, A., Wang, L., Oba, T., Kawahata, H., Huang, C.Y., 2005. Paleoenvironmental changes in the northern area of the East China Sea during the past 42,000 years. Palaeogeography, Palaeoclimatology, Palaeoecology 219, 239–261.

Isono, D., Yamamoto, M., Irino, T., Oba, T., Murayama, M., Nakamura, T., Kawahata, H., 2009. The 1500-year climate oscillation in the midlatitude North Pacific during the Holocene. Geology 37 (7), 591–594.

Jennings, A.E., Knudsen, K.L., Hald, M., Hansen, C.V., Andrews, J.T., 2002. A mid-Holocene shift in Arctic sea ice variability on the East Greenland Shelf. The Holocene 12, 49–58.

Jian, Z., Wang, P., Saito, Y., Wang, J., Pflaumann, U., Oba, T., Cheng, X., 2000. Holocene variability of the Kuroshio current in the Okinawa Trough, northwestern Pacific Ocean. Earth and Planetary Science Letters 184, 305–319.

Jin, Z., Wu, J., Cao, J., Wang, S., Shen, J., Gao, N., Zou, C., 2004. Holocene chemical weathering and climatic oscillations in north China: evidence from lacustrine sediments. Boreas 33, 260–266.

Kang, S.R., Lim, D.I., Kim, S.Y., 2010. Benthic foraminiferal assemblage of Seogwipo Formation in Jeju Island, South Sea of Korea: implication for late Pliocene to early Pleistocene cold episode in the northwestern Pacific margin. Quaternary International 225, 138–146.

Kawahata, H., Ohshima, H., Shimada, C., Oba, T., 2003. Terrestrial-oceanic environmental change in the southern Okhotsk sSa during the Holocene. Quaternary International 108, 67–76.

Kim, J.M., Kucera, M., 2000. Benthic foraminifer record of environmental changes in the Yellow Sea (Hwanghae) during the last 15,000 years. Quaternary Science Reviews 19, 1067–1085.

Kim, S.Y., Scourse, J., Marret, F., Lim, D.I., 2010. A 26,000-year integrated record of marine and terrestrial environmental change off Gabon, west equatorial Africa. Palaeogeography, Palaeoclimatology, Palaeoecology 297, 428–438.

Kim, S.Y., Lim, D.I., Cho, H.J., 2012. Dinoflagellate cyst assemblages from the northern shelf sediments of the East China Sea: an indicator of marine productivity. Marine Micropaleontology 96–97, 75–83.

Kong, G.S., Lee, C.W., 2005. Marine reservoir corrections (delta R) for southern coastal waters of Korea. Journal of the Korean Society of Oceanography [The Sea] 10, 124–128 (in Korean with English abstract).

Kong, G.S., Park, S.C., Han, H.C., Chang, J.H., Mackensen, A., 2006. Late Quaternary paleoenvironmental changes in the southeastern Yellow Sea, Korea. Quaternary International 144, 38–52.

Koizumi, I., Tada, R., Narita, H., Irino, T., Oba, T., Yamamoto, H., 2006. Paleoceanographic history around Tsugaru Strait between the Japan Sea and the Northwest Pacific Ocean since 30 cal Kyr BP. Palaeogeography, Palaeoclimatology, Palaeoecology 232, 36–52.

Lee, K.E., Kimoto, K., Kim, D.H., 2010. Glacial sea surface temperature of the East Sea (Japan Sea) inferred from planktonic foraminiferal assemblage. Geosciences Journal 14 (2), 127–134.

Lehmkuhl, F., 1997. Late Pleistocene, Late-glacial and Holocene glacier advances on the on the Tibetan Plateau. Quaternary International 38 (39), 77–83.

Li, B., Jian, Z., Wang, P., 1997. Pulleniatina obliquiloculata as a paleoceanographic indicator in the southern Okinawa Trough during the last 20,000 years. Marine Micropaleontology 32, 59–69.

Li, T.G., Sun, R.T., Zhang, D.Y., Liu, Z.X., Li, Q., Jiang, B., 2007. Evolution and variation of the Tsushima warm current during the late Quaternary: evidence from planktonic foraminifera, oxygen and carbon isotopes. Science in China Series D: Earth Sciences 50 (5), 725–735.

Lim, D.I., Park, Y.A., Choi, J.Y., Cho, J.W., Khim, B.K., 2000. Glauconite grains in continental shelf sediments around the Korean Peninsula and their depositional implications. Geo-Marine Letters 20, 80–86.
Lim, D.I., Kang, S.R., Yoo, H.S., Jung, H.S., Choi, J.Y., Kim, H.N., Shin, I.H., 2006. Late Quaternary sediments on the outer shelf of the Korea Strait and their paleoceanographic implications. Geo-Marine Letters 26, 287–296.
Lim, D.I., Xu, Z.K., Choi, J.Y., Kim, S.Y., Kim, E.H., Kang, S.R., Jung, H.S., 2011. Paleoceanographic changes in the Ulleung Basin, East (Japan) Sea, during the last 20,000 years: Evidence from variations in element composition of core sediments. Progress in Oceanography 88, 101–115.
Lin, H.L., Wu, S.M., Wang, C.H., 1996. A high-resolution hydrographic contrast between the East China Sea and the Japan Sea based on foraminiferal isotopic records for the late Holocene. TAO 7 (2), 225–238.
Liu, K., Sun, S., Jinag, X., 1992. Environmental change in the Yangtze River Delta since 12,000 years BP. Quaternary Research 38, 32–42.
Liu, J., Zhu, R., Li, T., Li, A., Li, J., 2007. Sediment-magnetic signature of the mid-Holocene paleoenvironmental change in the central Okinawa Trough. Marine Geology 239, 19–31.
Marret, F., Zonneveld, K.A.F., 2003. Atlas of modern organic-walled dinoflagellate cyst distribution. Review of Palaeobotany and Palynology 125, 1–200.
Marret, F., Maley, J., Scourse, J., 2006. Climatic instability in west equatorial Africa during the Mid- and Late Holocene. Quaternary International 150, 71–81.
Mason, O.K., Barber, V., 2003. A paleo-geographic preface to the origins of whaling: cold is better. In: McCartney, A.P. (Ed.), Indigenous Ways to the Present: Native Whaling in the Western Arctic. Canadian Circumpolar Institute Press, pp. 69–107.
Matthiessen, J., de Vernal, A., Head, M., Okolodkov, Y., Zonneveld, K., Harland, R., 2005. Modern organic-walled dinoflagellate cysts in Arctic marine environments and their (paleo-) environmental significance. Paläontologische Zeitschrift 79 (1), 3–51.
National Oceanic and Atmospheric Administration (NOAA), 1994. World Ocean Atlas.
Neff, U., Burns, S.J., Mangini, A., Mudelsee, M., Fleitmann, D., Matter, A., 2001. Strong coherence between solar variability and the monsoon in Oman between 9 and 6 kyr ago. Nature 411, 290–293.
Razjigaeva, N.G., Grebennikova, T.A., Ganzey, L.A., Mokhova, L.M., Bazarova, V.B., 2004. The role of global and local factors in determining the middle to late Holocene environmental history of the South Kuril and Komandar Islands, northwestern Pacific. Palaeogeography, Palaeoclimatology, Palaeoecology 209, 313–333.
Rho, K.C., 2009. Depositional history for the continental shelf of northern East China Sea since the Last Glacial Maximum. Ph.D. Thesis, Kunsan National University, Korea.
Saito, Y., Katayama, H., Ikehara, K., Kato, Y., Matsumoto, E., Oguri, K., Oda, M., Yumoto, M., 1998. Transgressive and highstand systems tracts and post-glacial transgression, the East China Sea. Sedimentary Geology 122, 217–232.
Sawada, K., Handa, N., 1998. Variability of the path of the Kuroshio Ocean current over the past 25,000 years. Nature 392, 592–595.
Schefuß, E., Schouten, S., Jansen, J.H.F., Damsté, J.S.S., 2003. African vegetation controlled by tropical sea surface temperatures in the mid-Pleistocene period. Nature 422, 418–421.
Shi, Y., Kong, Z., Wang, S., Tang, L., Wang, F., Yao, T., Zhao, X., Zhang, P., Shi, S., 1993. Mid-Holocene climates and environments in China. Global and Planetary Change 7, 219–234.
Sirocko, F., Garbe-Schönberg, D., McIntyre, A., Molfino, B., 1996. Teleconnection between the subtropical Monsoon and high-latitude climate during the last deglaciation. Science 272, 526–529.
Thompson, P.R., 1981. Planktonic foraminifera in the western north Pacific during the past 150,000 years: comparison of modern and fossil assemblages. Palaeogeography, Palaeoclimatology, Palaeoecology 35, 241–279.
Ujiié, H., Ujiié, Y., 1999. Late Quaternary course changes of the Kuroshio Current in the Ryukyu Arc region, northwestern Pacific Ocean. Marine Micropaleontology 37, 23–40.
Ujiié, Y., Ujiié, H., Taira, A., Nakamura, T., Oguri, K., 2003. Spatial and temporal variability of surface water in the Kuroshio source region, Pacific Ocean, over the past 21,000 years: evidence from planktonic foraminifera. Marine Micropaleontology 49, 335–364.
Wang, M., 1987. The spore-pollen groups of peatland on Ruoergai Plateau and paleobotany and paleoclimate. Scientia Geographica Sinica 7 (2), 147–155.
Wang, F., Fan, C.Y., 1987. Climatic changes in the Qinghai-Xizang (Tibetan) region of China during the Holocene. Quaternary Research 28, 50–60.
Wang, P., Zhang, J., Min, Q., 1985. Distribution of foraminifera in surface sediments of the East China Sea. In: Wang, P. (Ed.), Marine Micropaleontology of China. China Ocean Press, Beijing, pp. 34–69.
Wang, S.M., Yu, S.Y., Wu, R.J., Feng, M., 1990. The Daihai Lake – Lake Environment and Climate Change. Science and Technology University of China Press, Hefei.
Wang, S.M., Li, J.R., 1990. Lake sediment as an effective tool for historical climate: the case of Qinghai Lake and Daihai Lake. Chinese Science Bulletin 35, 54–56.
Wang, Y.J., Cheng, H., Edwards, R.L., He, Y., Kong, X., An, Z., Wu, J., Kelly, M.J., Dykoski, C.A., Li, X., 2005. The Holocene Asian monsoon: links to solar changes and North Atlantic climate. Science 308, 854–857.
Wanner, H., Solomina, O., Grosjean, M., Ritz, S.P., Jetel, M., 2011. Structure and origin of Holocene cold events. Quaternary Science Reviews 30, 3109–3123.
Weldeab, S., Schneider, R.R., Kölling, M., Wefer, G., 2005. Holocene African droughts relate to eastern equatorial Atlantic cooling. Geology 33 (12), 981–984.
Woodgate, R.A., Aagaard, K., Swift, J.H., Smethie Jr., W.M., Falkner, K.K., 2007. Atlantic water circulation over the Mendeleev Ridge and Chukchi Borderland from thermohaline intrusions and water mass properties. Journal of Geophysical Research 112, C02005.
Woodgate, R.A., Weingartner, T., Lindsay, R., 2010. The 2007 Bering Strait oceanic heat flux and anomalous Arctic sea-ice retreat. Geophysical Research Letters 37, L01602.
Xiang, R., Sun, Y.B., Li, T.G., Oppo, D.W., Chen, M.H., Zheng, F., 2007. Paleoenvironmental change in the middle Okinawa Trough since the last deglaciation: evidence from the sedimentation rate and planktonic foraminiferal record. Palaeogeography, Palaeoclimatology, Palaeoecology 243, 378–393.
Xiang, R., Yang, Z., Saito, Y., Fan, D., Chen, M., Guo, Z., Chen, Z., 2008. Paleoenvironmental changes during the last 8400 years in the southern Yellow Sea: benthic foraminiferal and stable isotopic evidence. Marine Micropaleontology 67, 104–119.
Xu, X., Oda, M., 1999. Surface-water evolution of the eastern East China Sea during the last 36,000 years. Marine Geolology 156, 285–304.
Yoo, D.G., Lee, C.W., Kim, S.P., Jin, J.H., Kim, J.K., Han, H.C., 2002. Late Quaternary transgaressive and highstand systems tracts in the northern East China Sea mid-shelf. Marine Geology 187, 313–328.
Yoo, K., Yoon, H.I., Kim, J.K., Khim, B.K., 2009. Sedimentological, geochemical and palaeontological evidence for a neoglacial cold event during the late Holocene in the continental shelf of th northern South Shetland Islands, West Antarctica. Polar Research 28, 177–192.
Zhang, Y.T., 1937. Water front change in the Daihai Lake and climatic implications. Geological Review 2, 263–266 (in Chinese with English abstract).
Zhang, J., Su, J.L., 2006. Nutrient dynamics of the China Sea: The Bohai Sea, Yellow Sea, East China Sea and South China Sea. In: Robinson, A.R., Brink, K.H. (Eds.), The Sea: The Global Coastal Ocean Interdisciplinary Regional Studies and Syntheses. Part A, Panreginal Syntheses and the Coasts of North and South America and Asia, vol. 14, pp. 637–671.